

Shahinoor Alam<sup>a\*</sup>, Mohammad Asaduzzaman Chowdhury<sup>b\*</sup>

Dhaka University of Engineering and Technology, Gazipur, Department of Mechanical Engineering, Gazipur-1707, Bangladesh

\*Corresponding author: E-mail: <sup>a</sup>majshahin4282@gmail.com, <sup>b</sup>asadzmn2014@yahoo.com

Received (Otrzymano) 18.02.2021

## ANALYSIS OF RANDOMLY DISTRIBUTED PARTICLES AND MATRIX INTERFACES OF EPOXY-BASED MULTILAYERED COMPOSITES

In this study, the surface morphology of composites, the effect of the particle geometry like the size and shape of the filler materials, their dispersion efficiency and interfaces are analyzed by morphological characterization. According to the tensile tests, it was found that the composites fabricated with CuO exhibit increasing trends of tensile strength in all the experiments compared to that of the composites with TiO<sub>2</sub>, which is verified by the degree of composite crystallinity determined by the strong interfacial interaction as well as the size, shape and compactness of the filler particles as observed by SEM micrograph analysis using Mountains software. Evaluation of this analysis shows similar amplitude variations in all the PSD curves of the composites and indicate a fatigue-like behavior. The stable isotropic properties in the composite samples with CuO result in a better surface finish, which was also well defined in the analysis of its surface texture and density function. Due to all these positive correlations, a significant rising trend in tensile strength (55.50, 105.53 and 20.40%) was found in every composite modified with CuO in comparison to TiO<sub>2</sub>. The highest tensile strength of the fabricated composite incorporating the CuO functional filler was found to be 105.530%. Such composites with TiO<sub>2</sub> and CuO having a tensile strength of 117.9 and 141.95 N/mm<sup>2</sup> respectively, may be used for the interior design of aircraft, watercraft, offices, residences, car and sports accessories and others.

**Keywords:** functional fillers, particle size and shape, interface, epoxy composites, morphology

### INTRODUCTION

Over the last few years, many advanced characterization techniques have gradually been introduced for testing nano-, micro- and macro-scaled composite materials modified with different functional fillers, with the help of transposition and mathematical operations [1-2]. Notable development has also been made in applying these processes to analyze the interface between the matrix and the fiber (or particle) as well as the size and shape of particles, taking into consideration how the fiber, particle and the matrix material interact and function. Consequently, the solution helps manufacturers to select appropriate matrices, functional fillers and fibers for fabricating composites with the desired properties.

The particle size, shape and their interfaces in fabricated composites modified by functional fillers or reinforced by fibers play a significant role in the field of composites. These particles may be of different size and shape and are being used in various materials, leading to a reduced load in the matrix [3-5]. The interconnections between the reinforcing materials and the matrices have a specific impact on composite properties (morphological and mechanical). For homogeneous distribution of the load and stress transformation among functional fillers, fibers and the epoxy-matrix interfaces play a crucial role [6, 7]. If interfacial adhesion exists

between them, then the development of microcracks at the edge of the fiber or encompassing the particle of functional fillers is unavoidable. However, due to the presence of good adhesion among the epoxy, fiber and filler particles, these microcracks cannot propagate easily alongside the facet of the fibers and filler particles [8]. The effectiveness of these correlations depends on the components used in manufacturing the fiber, filler particles, and epoxy matrices [9-10].

Many leading compositions and manufacturing techniques have been developed to fabricate fibers, fillers and matrices to meet the desired requirements as composite materials continue to play a significant role in their broad applications in the field of aerospace to biomedical engineering [11-13]. The mechanical and tribological properties are significantly enhanced due to the addition of silicon carbide as reinforcement in polymer-based composite materials [14]. Their improved properties established them as prime materials in the aviation industry, where these composites require precise drilling for assembly purposes and other applications [15, 16].

A group of parameters is generally responsible for the characterization of nanocomposites. Nevertheless, the size and shape of the filler particles, their interfaces and dispersion efficiency play a crucial role in deter-

mining the behavioral characteristics of composites. The adhesion performance between nanofibers and the matrix is enhanced owing to the increased aspect ratio, the projected surface area and the decreasing diameter of the fibers, which ultimately lead to the improved mechanical performance of composites [17]. By means of the homogeneous dispersion technique of nanocellulose in a matrix of starch, the tensile strength can be raised in bio-nanocomposites [18]. The fragile bond between the filler and matrix may lead to crack formation, which ultimately leads to the mechanical failure of composites [19].

Furthermore, the quality of the interfaces depends upon better adhesion properties between the filler and the matrix, which is the outcome of different processes (diffusion, attraction, chemical reaction, interlocking etc.) happening at the time of composite fabrication [20]. Surface uniformity is improved if SiC particles (99.5% purity and approximate size of 37 microns) are incorporated in a polymer matrix composite (PMC) as reinforcement. This ultimately leads to great improvement in the machinability of a fibrous composite material. In both the different evolution (DE) and base algorithm (BA) approaches, the material removal rate (MRP) is enhanced (8.08 and 7.9% respectively) compared to Taguchi's methodology (TM) [21].

Therefore, investigation of the types of fiber, matrix and particle (size and shape) is necessary to know how functional fillers and fibers are incorporated into the matrix material to ensure proper reinforcement of composites. Furthermore, to bring synergism to particle distribution and to create effective bonding between the matrix, fiber and functional particles, some physical and chemical modifications are also needed to be pursued [22-28]. With this background, this paper concerns the fabrication of composites using  $\text{CaCO}_3$ ,  $\text{Al}_2\text{O}_3$ ,  $\text{MgO}$ ,  $\text{TiO}_2/\text{CuO}$  functional fillers. The primary aim of this analysis is to evaluate the effect of the particle size, shape and interfaces of functional fillers in composites and the effects on their mechanical properties, particularly the tensile strength, aided by Mountains

Software analysis of SEM micrographs of composite samples. Additionally, the particle distribution, their dispersion efficiency, and synergism of the functional fillers in the matrix in addition to their interrelationship with the glass fiber are ascertained by investigating the microstructures of the composite samples.

## EXPERIMENTAL PROCEDURE

### Materials and Fabrication Process

Epoxy resin (LY556), E-type woven glass fiber, hardener (araldite HY951) and functional fillers ( $\text{CuO}/\text{TiO}_2$ ,  $\text{MgO}$ ,  $\text{Al}_2\text{O}_3$  and  $\text{CaCO}_3$ ) were used to fabricate the desired composite specimens. Different percentages of materials as presented in Tables 1 and 2 were applied during the fabrication process of the composites [29]. The wet hand lay-up technique was used to fabricate the composites by applying a similar compression pressure. Glass fiber mats were initially cut to a size of  $200 \times 150 \text{ mm}^2$ . Then the epoxy (LY556) and hardener (HY951) were mixed together at the ratio of 10:1 to prepare the matrix. Functional fillers (powder particles) of various wt.% were gradually added to the mixture according to Tables 1 and 2. The mixture was stirred with a magnetic stirrer for a period of 10-15 min to achieve the desired homogeneity. The mold was then prepared and OHP sheets were placed on the floor. For easy removal of the composite from the OHP sheet, wax was applied to it before hand. In order to increase the robustness, the prepared mixture was then poured in the mold. The fiber mat is placed the as the initial surface and is uniformly embedded on the OHP sheet with a roller. Then the matrix mixture was placed on the initial mat surfaces and rolled on it. Another layer of fiber mats was then placed on the initial surface, and the matrix mixture was applied on it uniformly by rolling. To obtain the required thickness, five consecutive layers were then produced. The prepared laminates were kept for curing in atmospheric conditions for two days [30].

TABLE 1. Composite composition in Experiment 1

Composite	Fiber layer number & sequence	Epoxy [wt.%]		Woven glass fiber [wt.%]	Functional fillers [wt.%]				
		Resin (LY556)	Hardener (HY951)		$\text{CaCO}_3$	$\text{Al}_2\text{O}_3$	$\text{MgO}$	$\text{TiO}_2$	Total
S1	G/G/G/G/G	35.00	5.00	55.00	1.25	1.25	1.25	1.25	5.00
S2	G/G/G/G/G	33.00	4.00	53.00	2.50	2.50	2.50	2.50	10.00
S3	G/G/G/G/G	31.00	3.00	51.00	3.75	3.75	3.75	3.75	15.00

TABLE 2. Composite composition in Experiment 2

Composite sample	Fiber layer sequence	Epoxy [wt.%]		Woven glass fiber [wt.%]	Functional fillers [wt.%]				
		Resin (LY556)	Hardener (HY951)		$\text{CaCO}_3$	$\text{Al}_2\text{O}_3$	$\text{MgO}$	$\text{CuO}$	Total
S4	G/G/G/G/G	35.00	5.00	55.00	1.25	1.25	1.25	1.25	5.00
S5	G/G/G/G/G	33.00	4.00	53.00	2.50	2.50	2.50	2.50	10.00
S6	G/G/G/G/G	31.00	3.00	51.00	3.75	3.75	3.75	3.75	15.00

### Scanning Electron Microscopy (SEM)

A Hitachi SU-1510 SEM was used to examine the microstructure of the composites. The fabricated composite samples were designed according to the ASTM standard D5299. The morphological properties of the composites were analyzed by means of the above mentioned microscope. The produced samples

were properly cleaned, air-dried and were prepared to observe by SEM. Thereafter, a thin and small-sized platinum film was evaporated on the composite specimens so as to increase the conductivity before taking the micrographs. With the same setup, six similar micrographs of the composites were taken as shown in Figure 1.

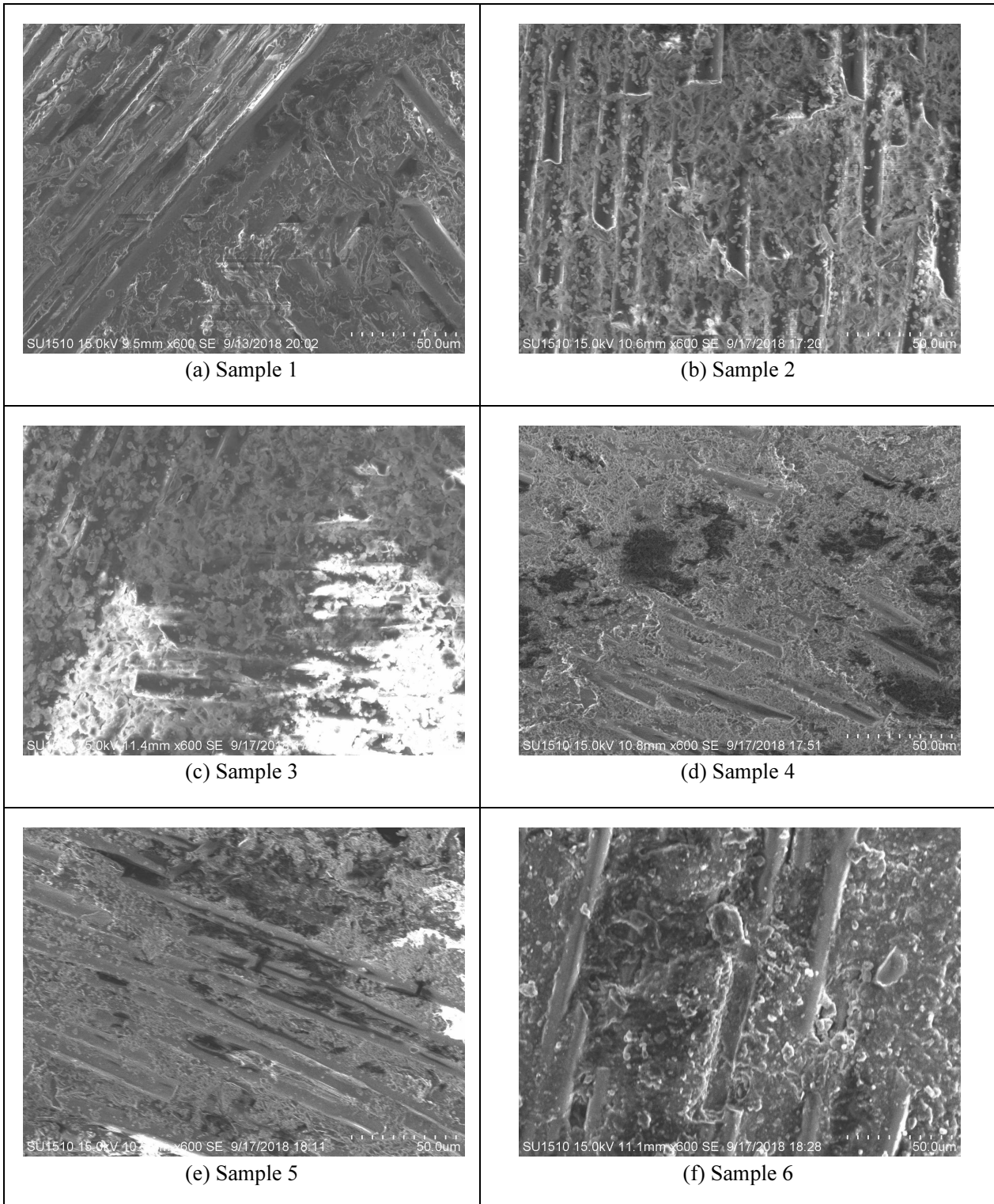


Fig. 1. SEM micrographs of all composite samples

## Tensile Strength Test

Composite specimens were prepared as per the ASTM D638 (ISO 527-2-1B) standard. Tensile testing was performed by a M350-10 (Testometric) twin column range universal testing machine (Fig. 2).



Fig. 2. Testometric machine and specimens for tensile strength test: a) specimen loading arrangement in Testometric machine, model M350-10, b) specimens after tensile test (ASTM D638)

The machine operated at the speed of 1 mm/min for this test at ambient temperature. The tensile strengths of the composites were recorded automatically (Table 3). Other mechanical properties of the composites were also considered, as determined in previous research work (Table 4) [30].

## Surface Roughness

The roughness values of the prepared composites were measured by a Taylor Hobson Surtronic S-128 surface roughness tester (Fig. 3). The recorded values are shown in Figure 4 and Table 5.

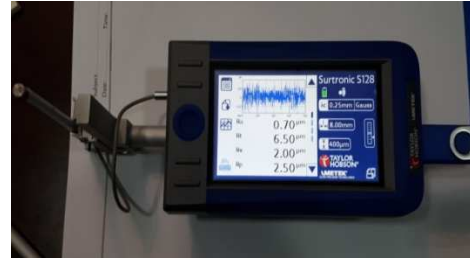


Fig. 3. Surface roughness tester (Surtronic S-128), Taylor and Hobson

## RESULTS AND DISCUSSION

### Mountains Software Analysis of SEM micrographs

SEM micrograph analysis was conducted to study the morphology of the composites and visualize the homogeneous distribution of the functional fillers using Mountains software. Notable variations in the uniformity of the functional fillers and internal structures were found (Figs. 5-12).

The entire specimen (Fig. 1) shows homogeneous distribution and uniformity of the fiberglass in all the samples. The composites fabricated with CuO exhibit the accepted tolerance limit in all the instances of samples 4, 5, and 6.

Edge detection is a fundamental tool for feature detection and feature extraction through image processing, machine vision and computer vision. This technique identifies and differentiates the genuine and in consistent edge pixels of the texture on the surface [31].

TABLE 3. Variations in tensile strength for difference of functional fillers

Composite specimen	Epoxy [wt %]		Woven glass fiber [wt %]	Functional fillers [wt.%]					Tensile strength [N/mm <sup>2</sup> ]	Variation in tensile strength [%]
	Resin (LY556)	Hardener (HY951)		CaCO <sub>3</sub>	Al <sub>2</sub> O <sub>3</sub>	MgO	TiO <sub>2</sub>	CuO		
S1	35.00	5.00	55.00	1.25	1.25	1.25	1.25	-	72.800	55.500
S4	35.00	5.00	55.00	1.25	1.25	1.25	-	1.25	113.200	
S2	33.00	4.00	53.00	2.50	2.50	2.50	2.50	-	65.050	105.530
S5	33.00	4.00	53.00	2.50	2.50	2.50	-	2.50	133.700	
S3	31.00	3.00	51.00	3.75	3.75	3.75	3.75	-	117.900	20.400
S6	31.00	3.00	51.00	3.75	3.75	3.75	-	3.75	141.950	

TABLE 4. Different mechanical properties of composite specimens

Experiment	Composite specimen	Impact strength [J/m]	Flexural strength [N/mm <sup>2</sup> ]	Stiffness [N/mm <sup>2</sup> ]	Tensile strength [N/mm <sup>2</sup> ]
Experiment 1	S1	796.3075	198.238	1686.174	72.700
	S2	534.9007	88.941	2323.361	65.045
	S3	741.3225	169.544	1741.334	117.886
Experiment 2	S4	755.1055	179.632	2106.130	113.080
	S5	957.0081	110.259	2565.205	133.666
	S6	837.2154	214.732	2819.752	141.879

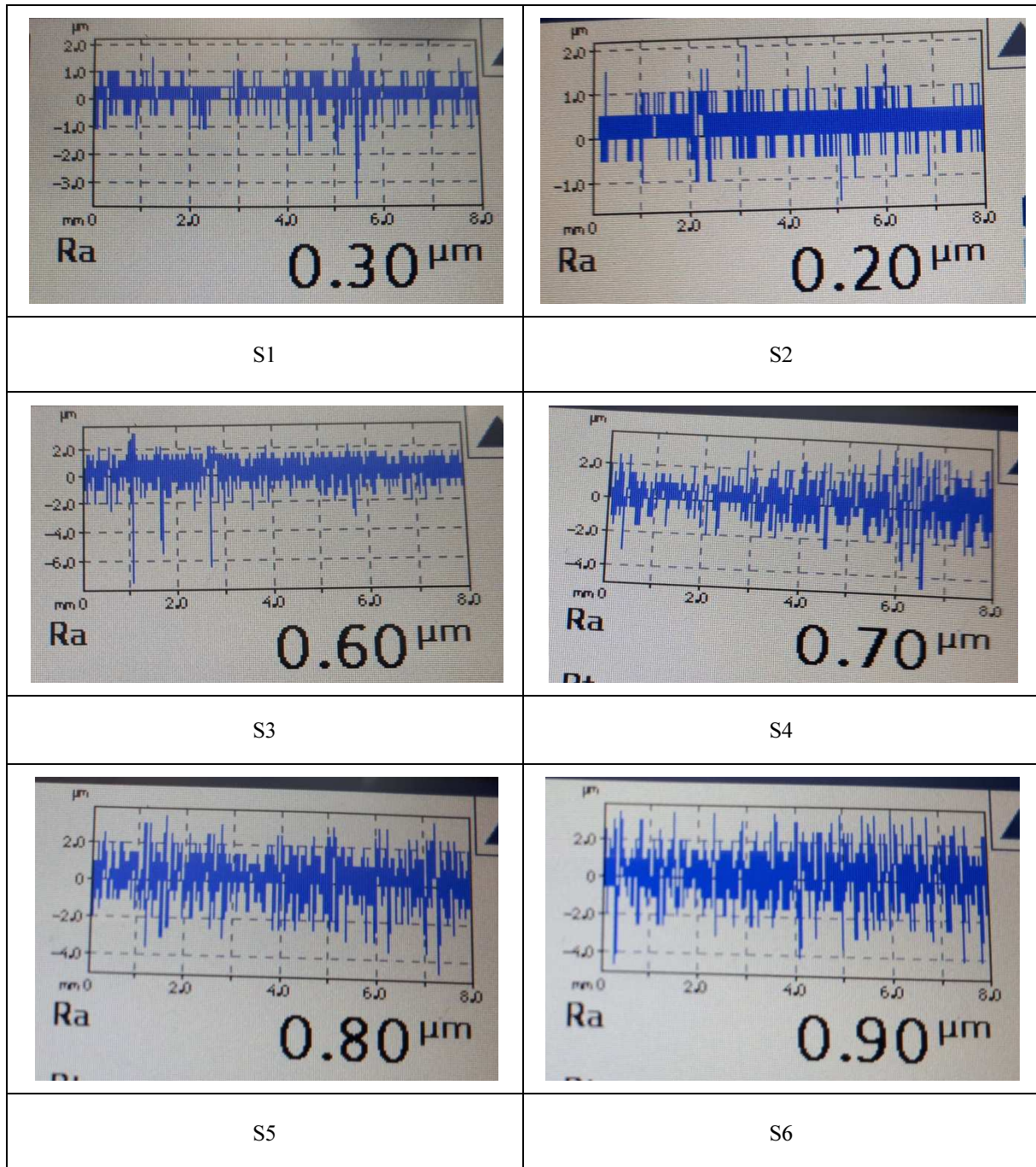


Fig. 4. Surface roughness profile curve

TABLE 5. Surface roughness (Ra) data of composite specimens

Experiment	Composite specimen	Measuring data 1 [ $\mu\text{m}$ ]	Measuring data 2 [ $\mu\text{m}$ ]	Measuring data 3 [ $\mu\text{m}$ ]	Average roughness [ $\mu\text{m}$ ]
Experiment 1	S1	0.30	0.30	0.30	0.30
	S2	0.20	0.20	0.20	0.20
	S3	0.50	0.60	0.70	0.60
Experiment 2	S4	0.60	0.80	0.70	0.70
	S5	0.70	0.90	0.80	0.80
	S6	1.00	0.90	0.80	0.90

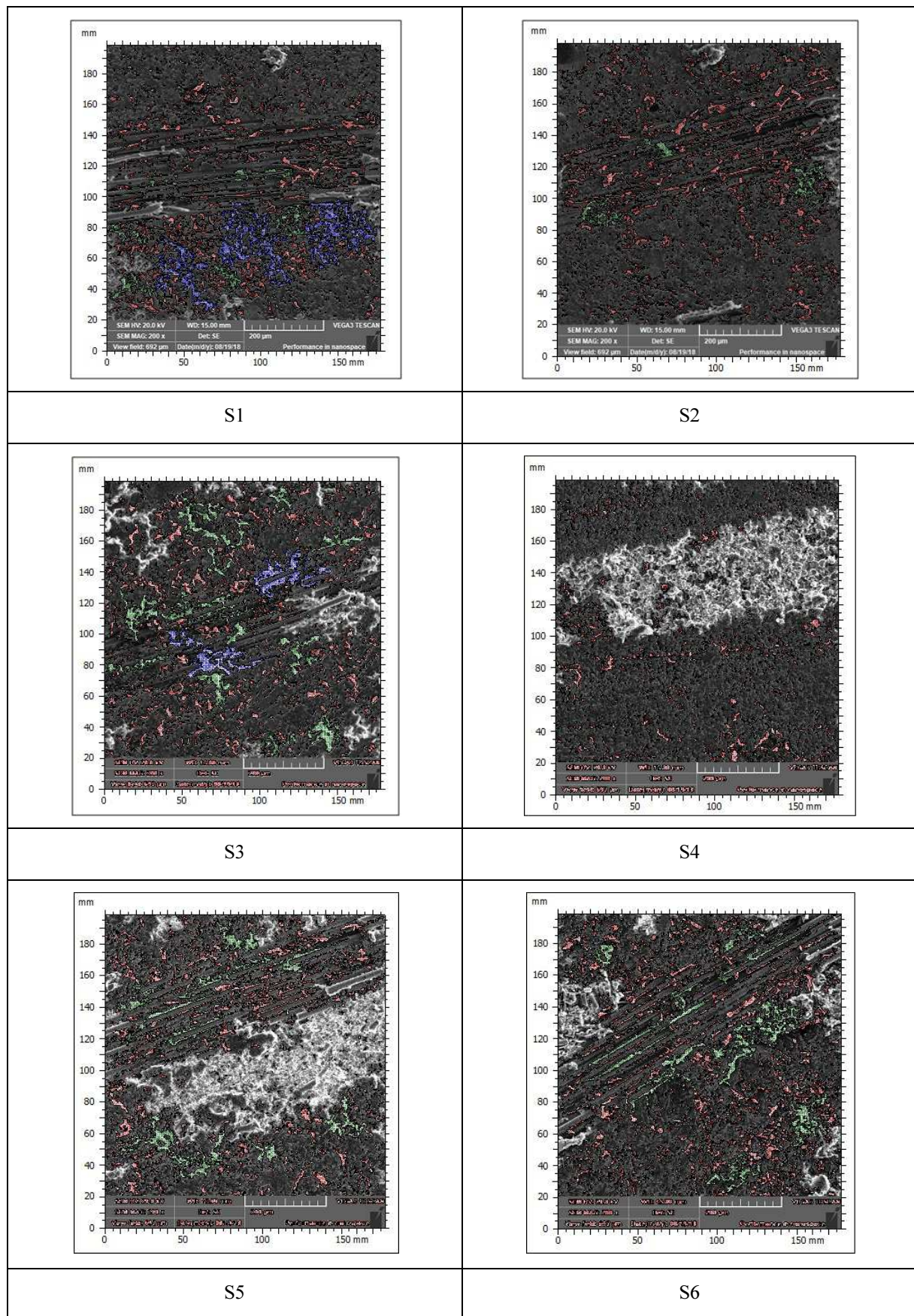


Fig. 5. Filler particle geometry (size and shape)



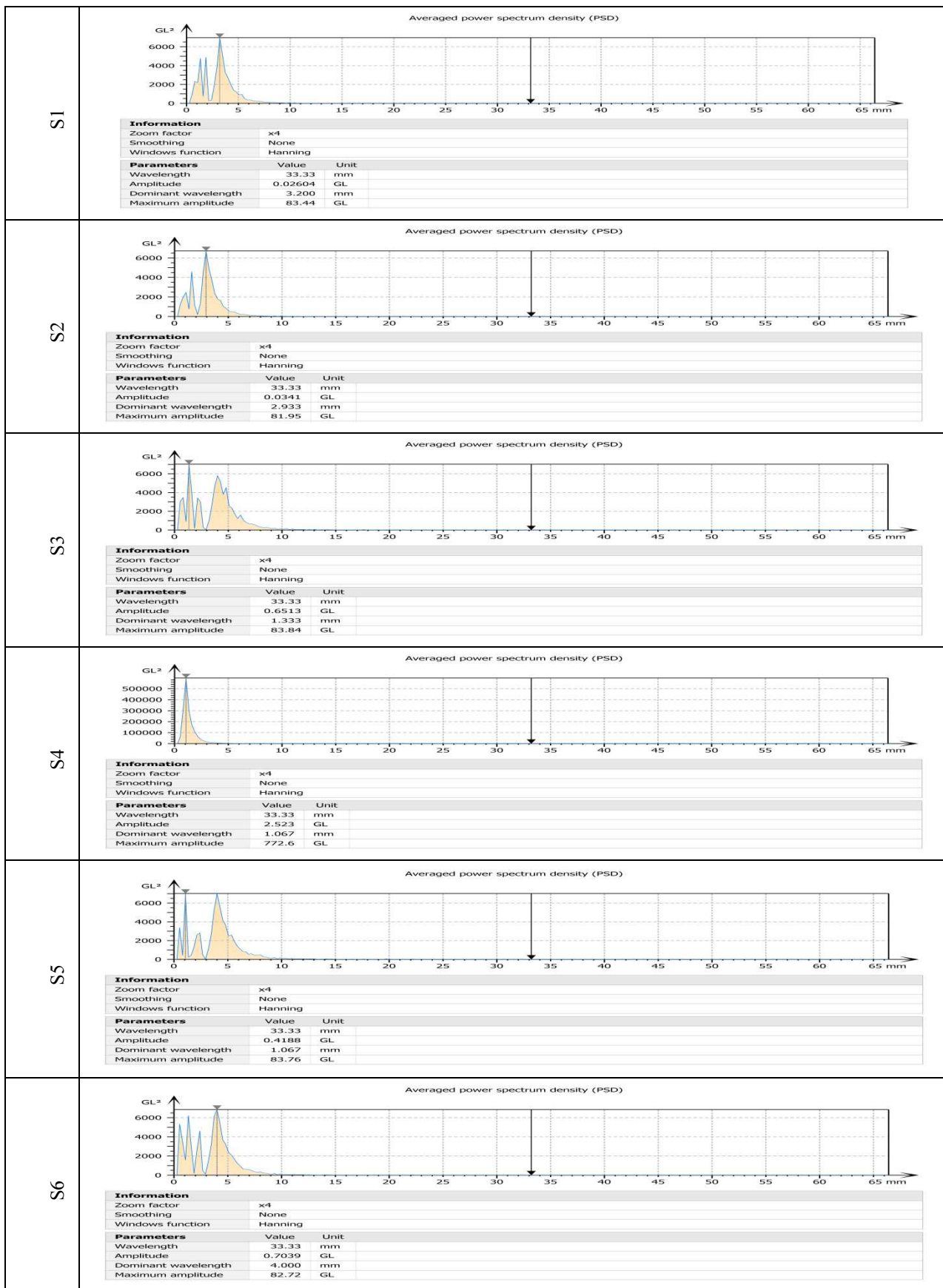


Fig. 7. Average power spectrum density (PSD) of composite specimens

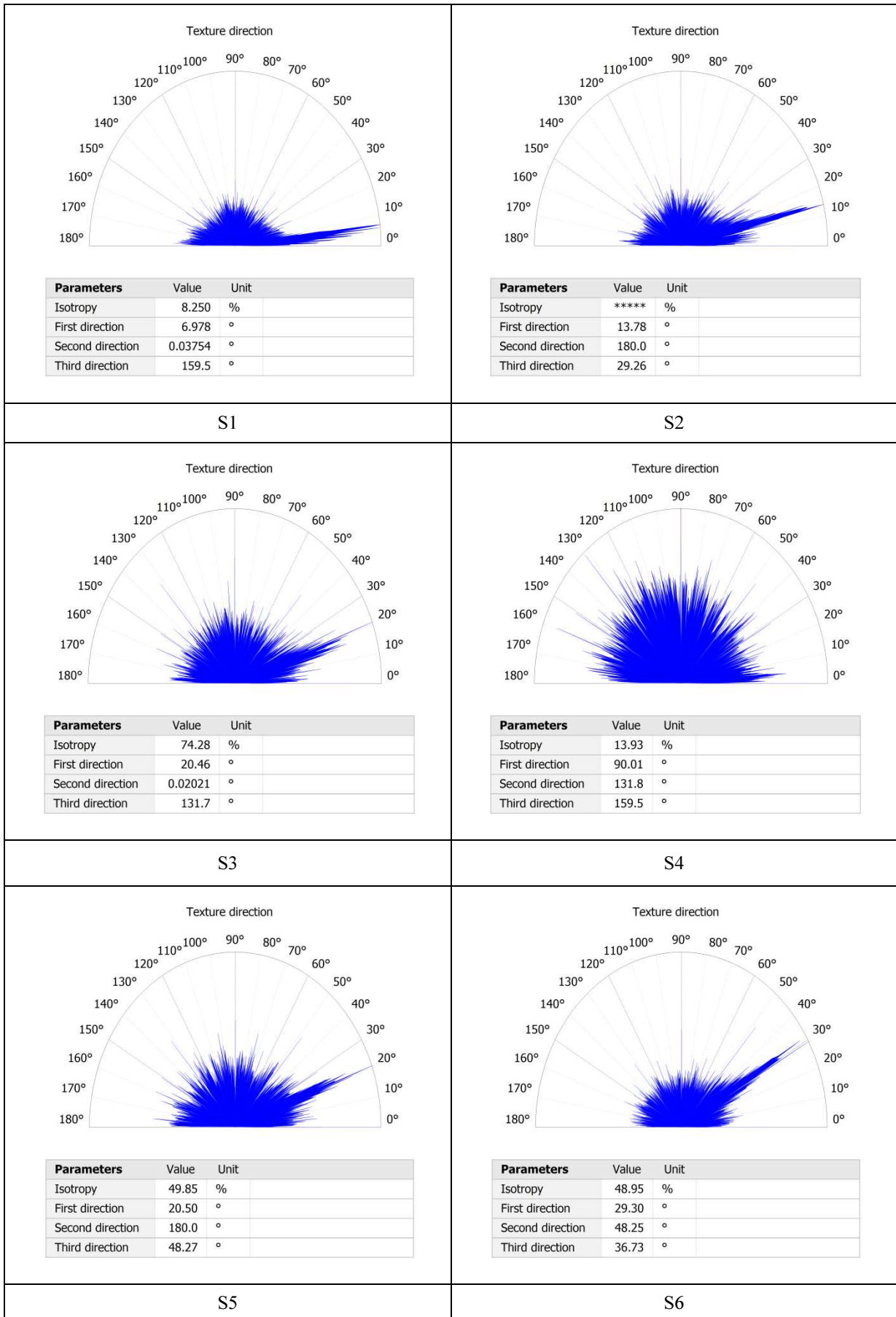


Fig. 8. Texture direction of composite specimens

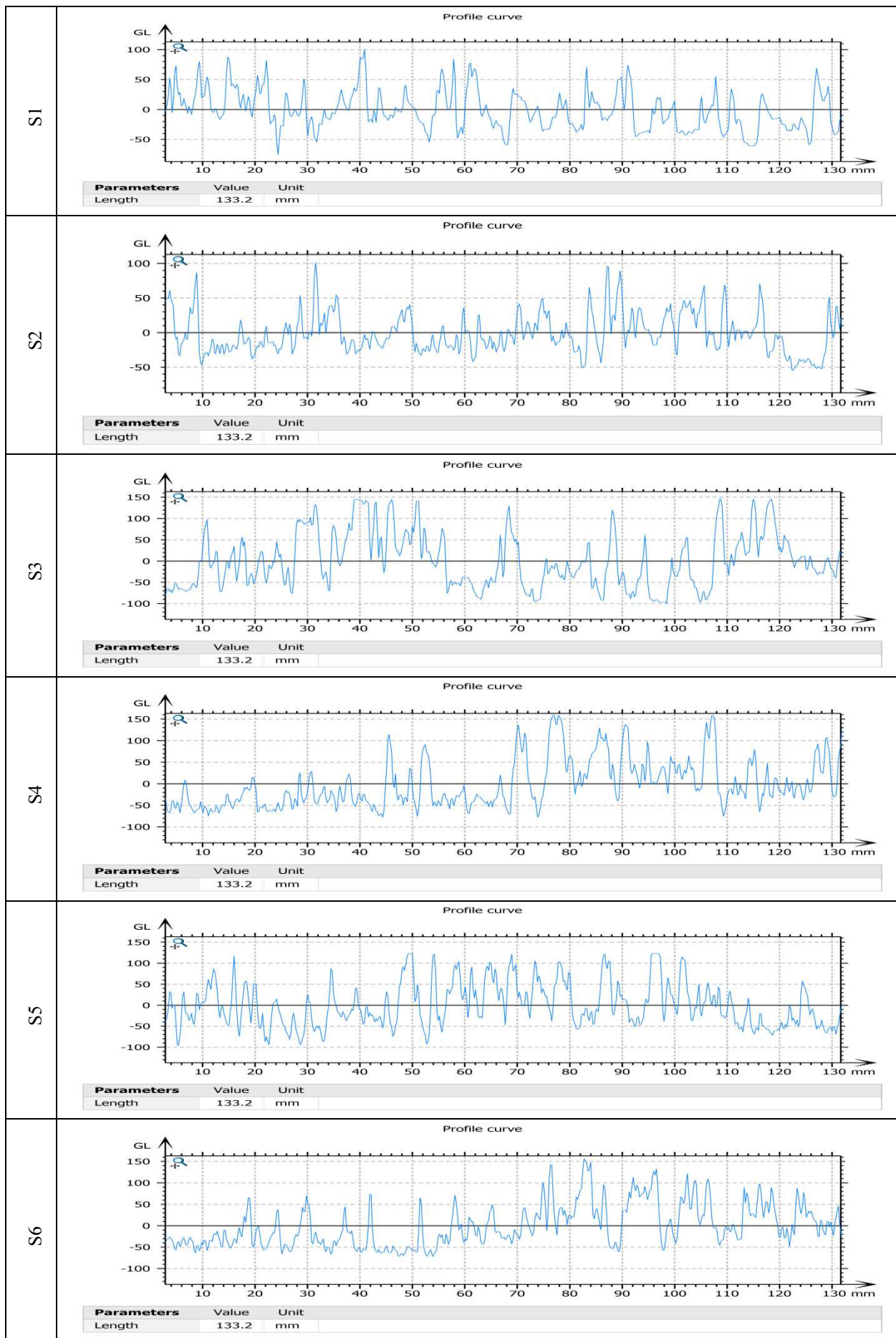


Fig. 9. Composite specimen profile curve

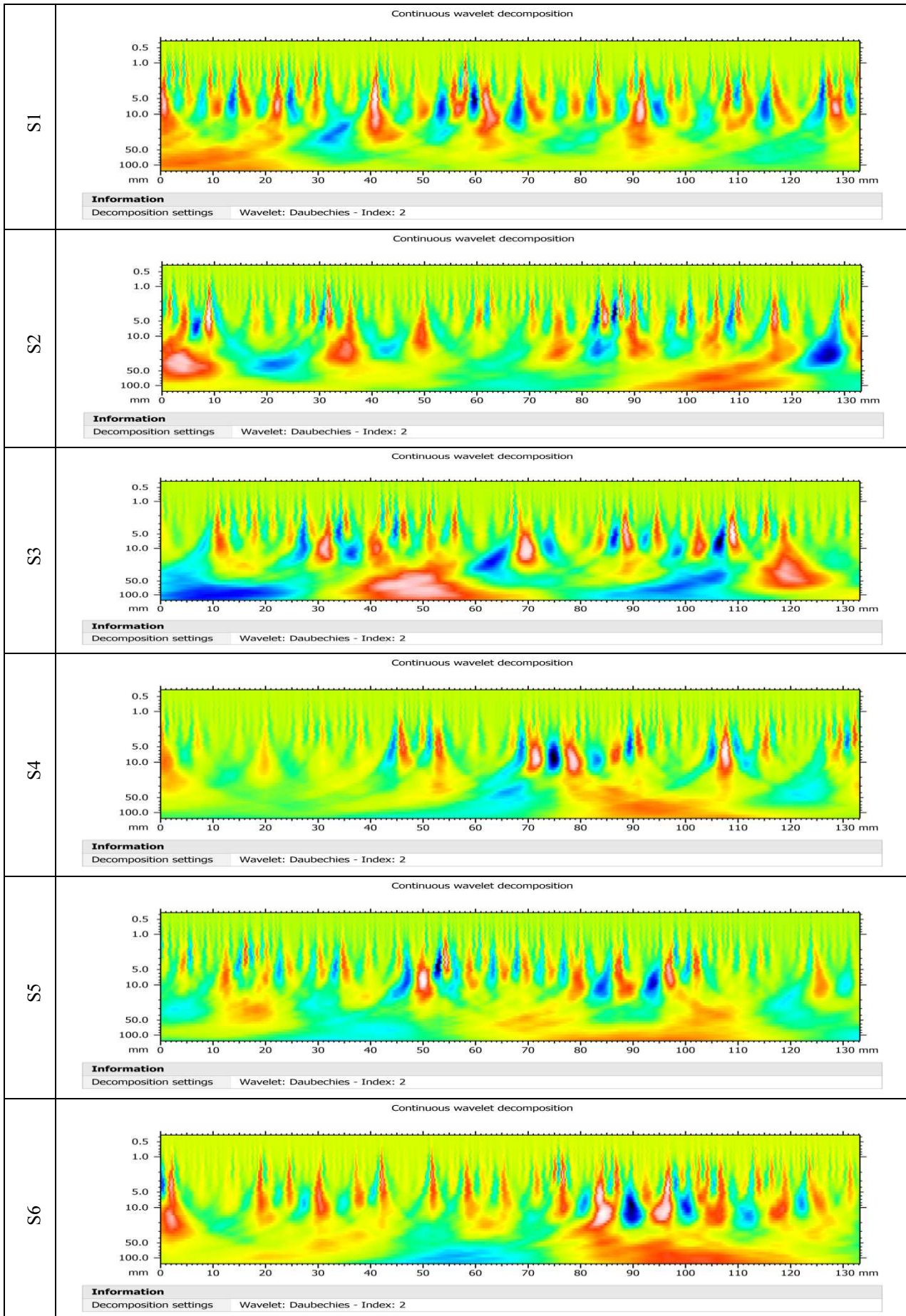


Fig. 10. Continuous wavelet decomposition of composite specimens

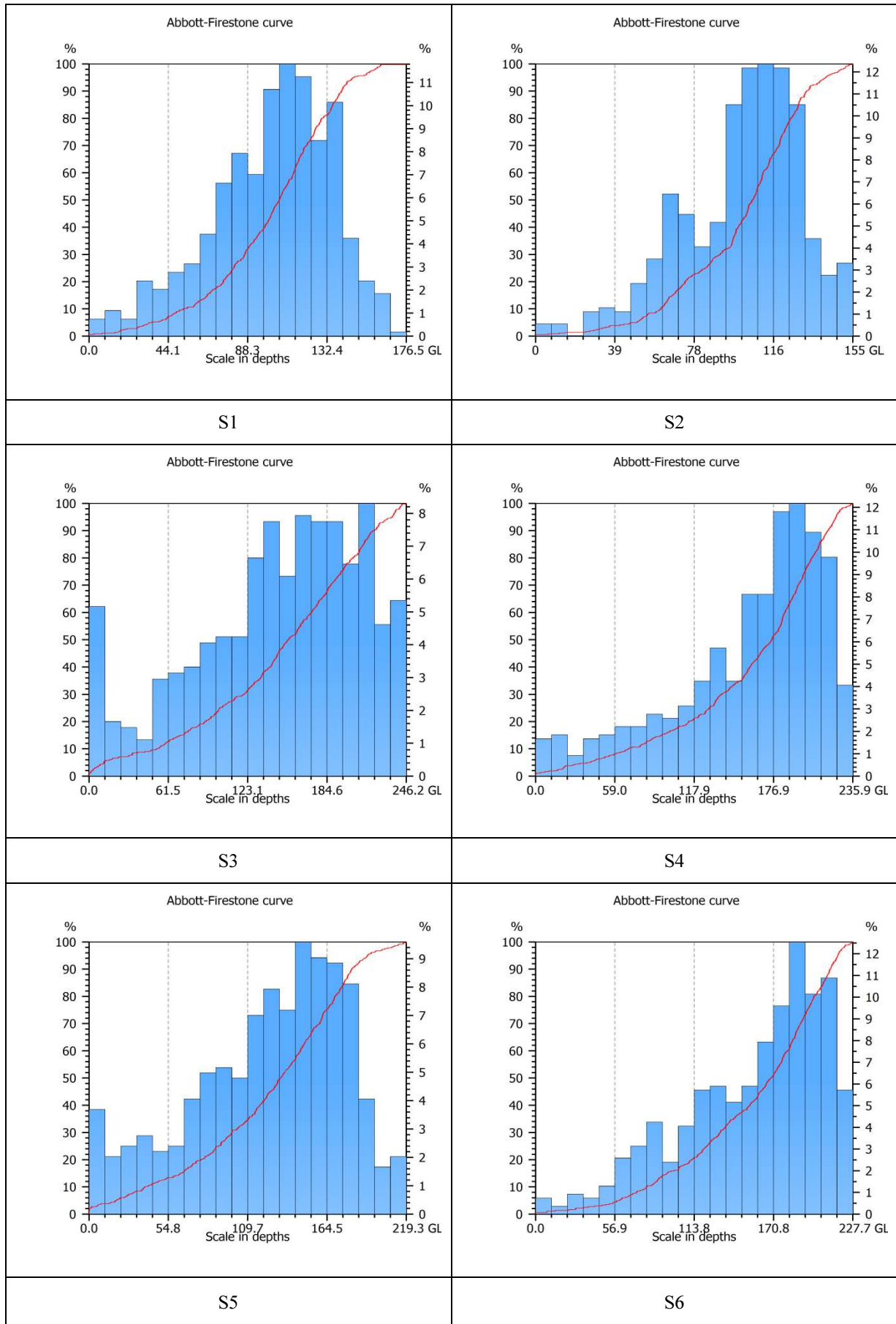


Fig. 11. Abbott-Firestone curve of composite specimens

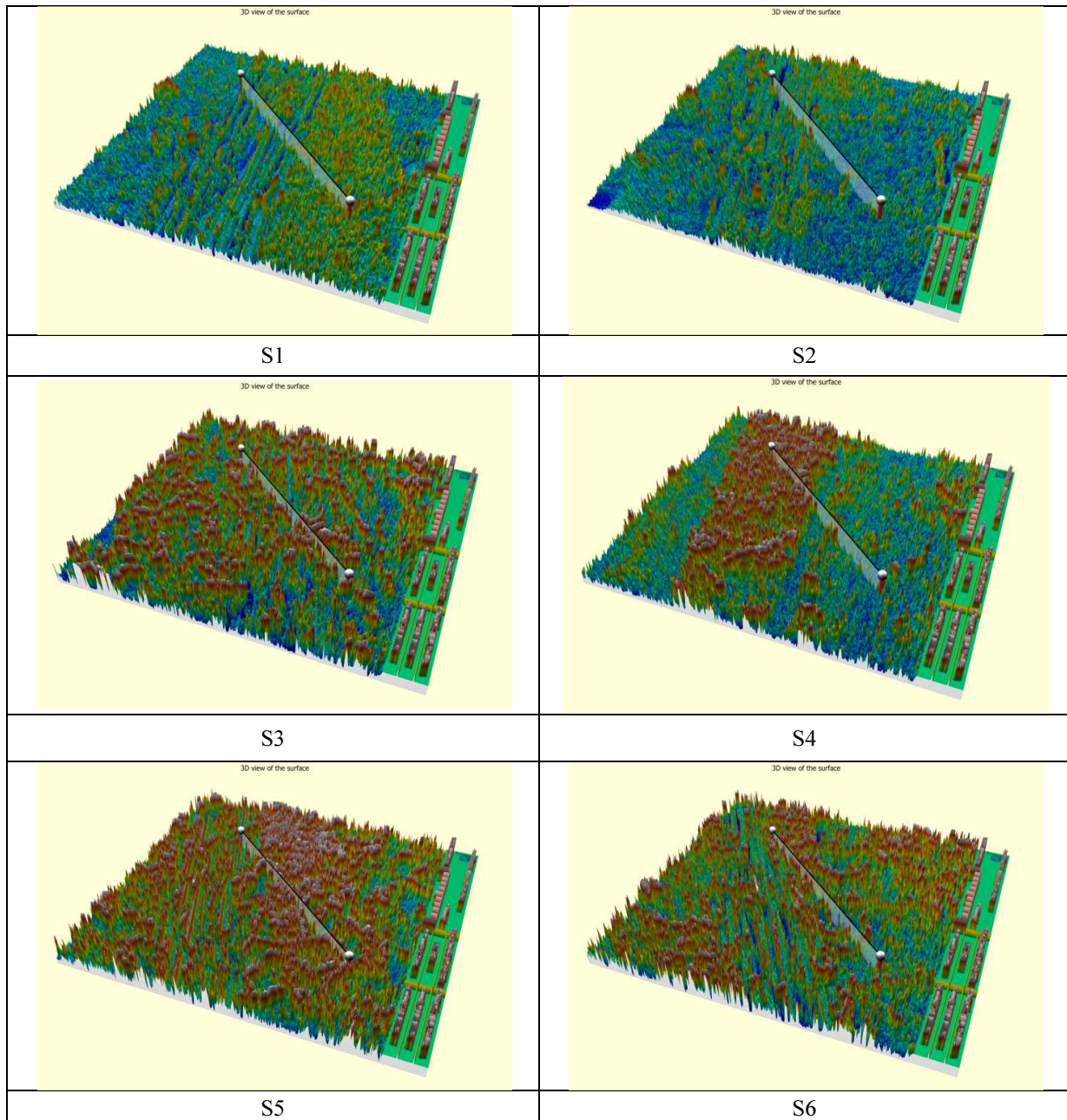


Fig. 12. 3D view of all composite specimens

To obtain an accurate size distribution from the micrographs, hundreds of particles were taken into account. Generally, the particle size is measured manually, which is very tiresome and painstaking. Moreover, human interference may affect manual measurement [32]. Therefore, scientific and more reliable methods are required to measure the particle size [33]. The edge detector helps to create a set of connected curves from the SEM micrograph, which indicates the boundaries of objects, the boundaries of surface markings as well as the curves of discontinuities in the surface. As a result, this detection technique reduces the data and filters out information which is less relevant for preserving the important structural properties of a micrograph. When the edge detection technique becomes successful, the interpretation of information in the original micrograph becomes significantly easier [34].

From Figure 5 and Table 6, it is observed that the compactness as well as tensile strength of the composites increased due to the growing aspect ratio of its functional fillers. This is noticeable in the composites fabricated with CuO, but it shows some abnormality in the case of the composites prepared with TiO<sub>2</sub>. This may be caused by the creation of unexpected voids and inadequate adhesion among the epoxy, functional fillers and glass fibers as depicted in composite specimen S2. Similarly, with an increasing mean equivalent diameter and projected area of the filler particles (as shown in Fig. 6 and Table 7), the good interfaces of the fiber and particles and good adhesion between them are seen. As a result, the composite fabricated with CuO exhibits better mechanical properties than that with TiO<sub>2</sub>.

TABLE 6. Particle size and shape of composite samples

Composite sample	Mean projected area [mm <sup>2</sup> ]	Mean diameter [mm]	Aspect ratio	Angle of maximum diameter [°]	Volume from threshold [mm <sup>3</sup> ]	Roundness	Compactness
S1	3.596	0.5476	1.793	1.731	476.5	0.5977	0.6787
S2	1.366	0.4175	1.663	4.202	170.2	0.6085	0.7775
S3	3.184	0.5803	1.720	2.675	513.3	0.6041	0.7740
S4	1.941	0.4032	1.646	1.404	298.2	0.6077	0.7771
S5	2.543	0.5104	1.701	4.354	517.4	0.6044	0.7742
S6	2.514	0.5522	1.784	6.973	411.2	0.6013	0.7716

The strength of the difference in energy protection by composites is determined by power spectral density (PSD) as a function of frequency. The amplitude differences shown in Figure 7 and Table 8 illustrate the fatigue of the materials, which is almost the same for all the prepared composites except Specimen 4 (amplitude 2.52300 GL). This may be caused by the agglomeration of some filler that does not achieve synergism during fabrication of the composite.

TABLE 7. Particle parameters of composite samples by edge detection method

Composite sample	Mean projected area [mm <sup>2</sup> ]	Mean equivalent diameter [mm]	Mean form factor	Mean orientation [°]
S1	96.61	10.78	0.3777	79.27
S2	103.7	11.13	0.3865	72.11
S3	115.3	11.59	0.4027	76.67
S4	100.0	10.92	0.4164	101.6
S5	94.58	10.62	0.3827	74.80
S6	107.1	11.29	0.3803	67.67

TABLE 8. Average power spectrum density (PSD) of composite samples

Composite sample	Wavelength [mm]	Amplitude [GL]	Dominant wavelength [mm]	Maximum amplitude [GL]
S1	33.33	0.02604	3.200	83.44
S2	33.33	0.03410	2.933	81.95
S3	33.33	0.65130	1.333	83.84
S4	33.33	2.52300	1.067	772.60
S5	33.33	0.41880	1.067	83.76
S6	33.33	0.70390	4.000	82.72

Due to the difference in texture directions, particle distributions, particle size and shape of CuO and TiO<sub>2</sub>, a difference in isotropy exists between the CuO and TiO<sub>2</sub> composites. The orientation of the reinforcing phase also affects the isotropy of the system. If the reinforcing particles have the same shape and dimensions in all directions (for example powders), the composites behave basically as an anisotropic material and therefore, their properties are the same in all directions. On the other hand, systems with cylindrical reinforcement (fibers) exhibit an isotropic properties [35]. In the case

of the composite sample with TiO<sub>2</sub>, the variations in the anisotropic properties are very dramatic, whereas in the composite sample with CuO, the variation is less (Fig. 8 and Table 9). This ultimately signifies that the composites fabricated with CuO exhibit improved mechanical properties in comparison with the composites modified with TiO<sub>2</sub>.

From Figure 1, it was found that specimens S4, S5 and S6 have adequate adhesion between the epoxy, functional fillers and glass fibers (Fig. 1d, 1e and 1f) as opposed to composite specimens S1, S2 and S3 (Fig. 1a, 1b and 1c), which were analyzed by the profile curve, wavelet decomposition and Abbott Fire Stone curve as shown in Figures 9-11. After being fractured, inadequate adhesion is observed between the fiber layer and the filler particles. It indicates unsatisfactory synergy among the components in their bonding state, which is potentially responsible for deterioration of the mechanical properties of composites. A useful ratio is observed among the compositions of the specimens in both Experiment 1 and 2. Nonetheless, the composition and synergy of Experiment 2 demonstrate an improved transformation and dispersion of stress in the composite samples (Figs. 12 and 13).

TABLE 9. Texture directions of composite samples

Composite samples	Isotropy [%]	First direction [°]	Second direction [°]	Third direction [°]
S1	8.250	6.978	0.03754	159.50
S2	-	13.780	180.000	29.26
S3	74.28	20.460	0.02021	131.70
S4	13.93	90.010	131.800	159.50
S5	49.85	20.500	180.000	48.27
S6	48.95	20.300	48.2500	36.73

The profile curves, wavelet decompositions and 3D views of the composites as shown in Figures 9-12 represent the entire images of the composites and indicate disintegration as per the orientation and defined scale. The development of wear and erosion of the functional particles is evaluated by the wavelet decomposition technique. The above mentioned figures illustrate that the composites fabricated with CuO exhibit less wear and erosion phenomena (S4, S5 and S6) than that of the composites with TiO<sub>2</sub> (S1, S2 and S3).

Among these composite samples, S6 showed a more dominant wave length because of its greater surface uniformity. This ultimately led to great improvement in the machinability of fibrous composite materials [21].

The roughness parameter represents the surface topography of the composite surface (Fig. 4 and Table 5). The Abbott-Firestone curve of a material and its parameters is one of the surface characterization techniques that best represents its functional properties. In this curve, the cumulative distribution of profile heights as a percentage of the material is graphically expressed. The Abbott-Firestone bearing curve makes the distribution of the heights of the peaks and depths of the valleys in the profile visible. If the functional characteristics of a surface are to be studied, the Abbott-Firestone curve is the suitable course of action [36]. The surface texture of the composite sample is the cumulative probability density function of the surface profile height, which is determined by integrating the profile trace with the help of the Abbott-Firestone curve (Fig. 11). Upon observing these profile traces, it is proved that the composites fabricated with CuO have a better surface texture and improved mechanical characteristics in comparison with the composites modified with the TiO<sub>2</sub> functional filler.

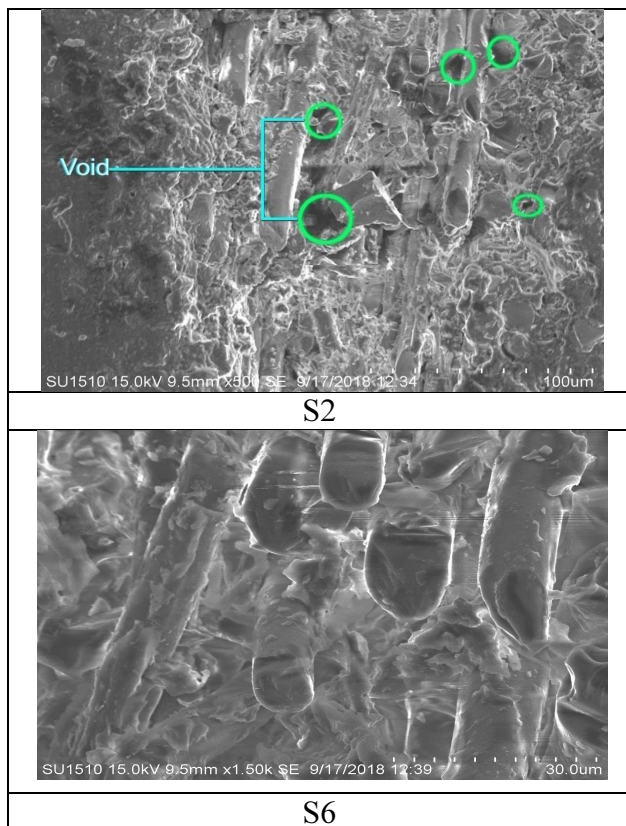


Fig. 13. SEM micrograph of composite samples 2 and 6

### Tensile strength

By adding functional fillers, a change in the tensile strength is observed, which is enhanced owing to the increasing amount of fillers in all the instances of Experiment 1 and 2 of the composite specimens

(Fig. 14). The differences in the filler particles is responsible for the growth in tensile strength. Particles having good bonding quality with their interfaces, uniform stress transformation and increasing diameter, projected area and aspect ratio can contribute substantially to improvement in the tensile strength of composites as confirmed by SEM and Mountains software (Figs. 1-12). The abnormality in Specimen 2 of Experiment 1 may be the result of inadequate adhesion among the epoxy, functional fillers, and glass fiber (Figs. 13 and 14).

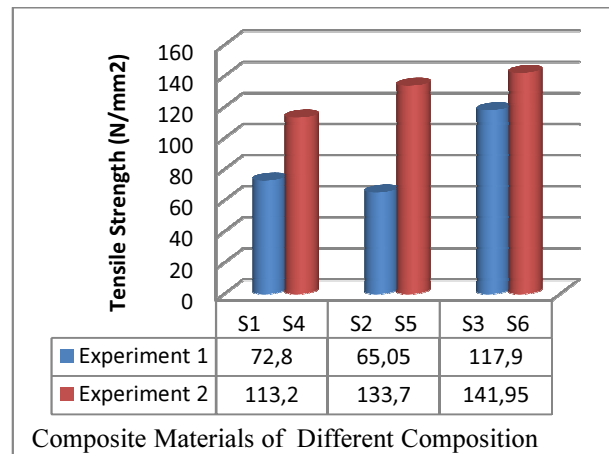


Fig. 14. Tensile strength due to variation of functional fillers

The unexpected formation of voids may also be one of the reasons for this deviation. A rising trend of the tensile strength (55.50, 105.53 and 20.40%) was noticed in the composites fabricated with the CuO functional filler compared to that of TiO<sub>2</sub> (Table 3). Other mechanical properties of the composite specimens (impact strength, flexural strength and stiffness) as determined in our previous research work also support the statement [37].

### CONCLUSIONS

To analyze the material morphology and understand the uniform distribution of the filler particles in the composite based on the SEM micrographs, two types of composites with varying filler materials (CaCO<sub>3</sub>, Al<sub>2</sub>O<sub>3</sub>, MgO and TiO<sub>2</sub>/CuO) with discrete weight ratios were successfully fabricated. The following conclusions can be drawn:

- With an increasing aspect ratio, the compactness of the functional fillers was found to increase, which is significant in the fabricated composites modified with CuO rather than TiO<sub>2</sub>.
- Similarly, with an increasing diameter and projected area of the filler particles, the bonding effect of the matrix, fibers and particles is enhanced, and improved adhesion among them is achieved.
- Variations in the amplitude were found to be almost the same for all the PSD curves, which indicates a nearly similar fatigue behavior of the composite

specimens except for Specimen 4. This may be caused due to the agglomeration of some functional fillers that do not achieve synergism in the fabricated composites.

- The isotropic properties are stable in the composite samples with CuO in comparison to that of TiO<sub>2</sub>, which indicates a better surface finish of the composites with CuO.
- The 3D view, profile cuve and wavelet decomposition phenomena acting on the particles reveal less wear and erosion exhibited by the fabricated composites modified by CuO than that of TiO<sub>2</sub>.
- The composites modified with the CuO functional filler have a comparatively rougher surface than that of the composites modified with TiO<sub>2</sub>, which is also distinct in the analysis of its surface texture and density function.
- Due to all the above positive correlations, a significant rising trend of the tensile strength (55.50, 105.53, and 20.40%) is noticed in every composite fabricated with the CuO functional filler compared to that of TiO<sub>2</sub>. The maximum increment in tensile strength of the composite fabricated with the CuO functional fillers was found to be 105.530%.
- The composites fabricated with TiO<sub>2</sub> and CuO having a tensile strength of 117.9 and 141.95 N/mm<sup>2</sup> respectively can be used for the interior design of aircraft, watercraft, offices, residences, car and sports accessories, and others.

## REFERENCES

- [1] Zhao Z., Dang H., Zhang C., Yun G.J., Li Y., A multi-scale modeling framework for impact damage simulation of tri axially braided composites, *Composites Part A* 2018, 110, 113-125.
- [2] Cranford S.W., de Boer J., Van Blitterswijk C., Buehler M.J., Materiomics: an -omics approach to biomaterials research, *Adv. Mater.* 2013, 25, 802-824.
- [3] De Silva R.T., Soheilmooghaddam M., Goh K.L., Wahit M.U., Abd bee H., Sharifah C.S.-P., Pasbakhsh P., Influence of the processing methods on the properties of poly(lactacid)/halloy site nanocomposites, *Polym. Compos.* 2016, 37, 861-869.
- [4] Goh K.L., Aspden R.M., Mathias K.J., Hukins D.W.L., Finite-element analysis of the effect of material properties and fiber shape on stresses in an elastic fiber embedded in an elastic matrix in a fiber-composite material, *Proceedings of the Royal Society of London* 2004, 2339-2352.
- [5] Fu S.Y., Feng X.Q., Lauke B., Mai Y.W., Effects of particle size, particle/matrix interface adhesion and particle loading on mechanical properties of particulate-polymer composites, *Compos. B Eng.* 2008, 39, 933-996.
- [6] De Silva R.T., Pasbakhsh P.G., Goh K.L., Mishnaevsky L., 3-D Computational Model of Poly (Lactic Acid)/halloy site Nanocomposites: Predicting Elastic Properties and Stress Analysis, *Polymer (United Kingdom)* 2014, 55.
- [7] Nath R.B., Fenner D.N., Galiotis C., The progressional approach to interfacial failure in carbon reinforced composites: elasto-plastic finite element modelling of interface cracks, *Compos. Appl. Sci. Manuf.* 2000, 31, 929-943.
- [8] Goh K.L., *Discontinuous-fiber Reinforced Composites, Fundamentals of Stress Transfer and Fracture Mechanics*, Springer-Verlag, 1st ed., London 2017.
- [9] Zabihi C., Ahmadi M., Nikafshar S., Preyeswary K.C., Naebe M., A technical review on epoxy-clay nanocomposites: structure, properties, and their applications in fiber reinforced composites, *Composites Part B* 2018, 135, 1-24.
- [10] Kausar A., Review on polymer/halloysite nanotube nanocomposite, *Polym. Plast. Technol. Eng.* 2018, 57, 548-564.
- [11] Lavagna L., Massella D., Pantano M.F., Bosia F., Pugnoand N.M., Pavese M., Grafting Carbon Nanotubes onto Carbon Fibers Doubles their Effective Strength and the Toughness of the Composite, *Composites Science and Technology* 2018.
- [12] Mittal G., Rhee K.Y., Miskovic-Stankovic V., Hui D., Reinforcements in multi-scale polymer composites: processing, properties, and applications, *Composites Part B* 2018, 138, 122-139.
- [13] Liu X., Liu D., Lee J.H., Zheng Q., Du X., Zhang X., Xu H., Wang Z., Wu Y., Shen X., Cui J., Mai Y.W., Kim J.K., Spider web-inspired stretchable graphene woven fabric for highly sensitive, transparent, wearable strain sensors, *ACS Appl. Mater. Interfaces* 2018, 11, 2282-229.
- [14] Latha P.S., Rao M.V., Investigation into effect of ceramic fillers on mechanical and tribological properties of bamboo-glass hybrid fiber reinforced polymer composites, *Silicon* 2018, 10(4), 1543-1550.
- [15] Rahamathullah I., Shunmugam M.S., Mechanistic approach for prediction of forces in micro-drilling of plain and glass-reinforced epoxy sheets, *Int. J. Adv. Manuf. Technol.* 2014, 75, 1177-1187.
- [16] Antil P., Modeling and multi-objective optimization during ECDM of silicon carbide reinforced epoxy composites, *Silicon* 2019, DOI: 10.1007/12633-019-00122-8.
- [17] Tonoli G.H.D., Joaquim A.P., Arsene M.-A., Bilba K., Savastano H., Performance and durability of cement based composites reinforced with refined sisal pulp, *Mater. Manuf. Process.* 2007, 22, 149-156.
- [18] Abrial H., Dalimunthe M.H., Hartono J., Efendi R.P., Asrofi M., Sugiarti E., Characterization of tapioca starch biopolymer composites reinforced with micro scalewater hyacinth fibers, *Starch/Staerke* 2018, 70, 1-8.
- [19] Ahamed A.R., Asokan P., Aravindan S., EDM of hybrid Al-SiCp-B4Cp and Al-SiCp-Glass pMMCs, *International Journal of Advanced Manufacturing Technology* 2009, 44, 5-6, 520-528.
- [20] Zhou Y., Fan M., Chen L., Interface and bonding mechanisms of plant fiber composites: an overview, *Compos. Part B Eng.* 2016, 101, 31-45.
- [21] Antil P., Singh S., Singh S., Prakash C., Pruncu C.L., Metaheuristic approach in machinability evaluation of silicon carbide particle/glass fiber-reinforced polymer matrix composites during electrochemical discharge machining process, *Measurement and Control* 2019, DOI: 10.1177/0020294019858216.
- [22] Miriyala S.M., Kim Y.S., Liu L., Grunlan J.C., *Macromol. Chem and Phys.*, Wiley Online Library, 2008, 209, 23, 2399-2409.
- [23] Chaturvedi S.K., An experimental investigation of tensile strength of glass composite materials with calcium carbonate (CaCO<sub>3</sub>) filler, *International Journal of Emerging Trends in Engineering and Development* 2012, 6(2), 303-309.
- [24] Devendra K., Rangaswamy T., Determination of mechanical properties of Al<sub>2</sub>O<sub>3</sub>, Mg(OH)<sub>2</sub> and SiC filled E-glass/epoxy composites, *International Journal of Engineering Research and Applications* 2012, 2028-2033.

- [25] Cao Y., Goda K., Shibata S., Development and mechanical properties of baggage fiber reinforced composites, *Advanced Composite Material*, Taylor and Francis 2007, 16, 4, 283-298.
- [26] Jacob M., Thomas S., Varughese K.T., Mechanical properties of sisal/oil palm hybrid fiber reinforced natural rubber composites, *Composite Science and Technology* 2004, 64, 955-965.
- [27] Hamdan M.H.M, Siregar J.P., Thomas S., Jacob M.J., Jafar J., Tezara C., Mechanical performance of hybrid woven jute-reselle-reinforced polyester composites, *Polymers and Polymer Composites* 2019, 27, 7, 407-418.
- [28] Magendran S.S., Khan F.S.A, Mubarak N.M., Khalid M., Walvekar R., Abdullah E.C., Nizamuddin S., Karri R.R., Synthesis of organic phase change materials by using carbon nanotubes as filler materials, *Nanostructures and Nano-objects* 2019, 19(100361).
- [29] Alam M.S., Chowdhury M.A., Water and brine absorption capacity of epoxy based glass fiber composite modified with  $\text{CaCO}_3\text{-Al}_2\text{O}_3\text{-MgO-TiO}_2\text{/CuO}$  filler materials, *Mater. Res. Express* 2019, 6(115311).
- [30] Alam M.S., Chowdhury M.A., Characterization of epoxy composites reinforced with  $\text{CaCO}_3\text{-Al}_2\text{O}_3\text{-MgO-TiO}_2\text{/CuO}$  filler materials, *Alexandria Engineering Journal*, 2020, DOI: 10.1016/j.aej.2020.07.017.
- [31] Lindeberg T., Edge detection and ridge detection with automatic scale selection, *International Journal of Computer Vision* 1998, 30(2), 117-154.
- [32] Lovell E.C., Scott J., Amal R.,  $\text{NiSiO}_2$  catalysts for the carbon dioxide reforming of methane: Varying support properties by flame spray pyrolysis, *Molecules* 2015, 20(3), 4594-4609.
- [33] Mang Y., Zhang. Z. Yin H., Me. T., Automatic deflection of particle size distribution by image analysis based on local adaptive carry edge detection and modified circular hough transform, *Micron* 2017, DOI. 10.1016/s.micron.2017.12.002.
- [34] en.wikipedia.org>wiki>Edge detection, extracted on 10 December 2020.
- [35] Rajeswari A., Jackcina S.C.E., Gopi S., Jayaraj K., Pius A., Characterization studies of polymer-based composites related to functionalized filler-matrix interface, *Interfaces in Particle and Fiber Reinforced Composites* 2020, 219-250, DOI:10.1016/b978-0-08-102665-6.00009-1.
- [36] Salcedo M.C., Coral I.B., Ochoa G.V., Characterization of surface topography with abbot firestone curve, *Contemporary Engineering Sciences* 2018, 11, 68, 3397-3407.
- [37] Alam M.S., Chowdhury M.A., Characterization of epoxy composites reinforced with  $\text{CaCO}_3\text{-Al}_2\text{O}_3\text{-MgO-TiO}_2\text{/CuO}$  filler materials, *Alexandria Eng. J.* 2020, DOI: 10.1016/j.aej.2020.07.01.